CrossMark

RESEARCH PAPER

Room-temperature sol–gel synthesis of organic ligand-capped ZnO nanoparticles

**Mirijam Zobel · Haimantee Chatterjee ·
Galina Matveeva ·
Ute Kolb · Reinhard B. Neder**

Abstract Powders of zinc oxide nanoparticles with individual particle sizes below 10 nm in diameter are readily produced in base-induced sol–gel processes from ethanolic solutions of zinc acetate dihydrate. These particles are covered with acetate molecules and without further stabilization, they grow when stored as a powder. Here, we present three organic ligands, which reproducibly stabilize individual particle sizes <5 nm within the agglomerated powders for extended periods of time, up to months. Citric acid and 1,5-diphenyl-1,3,5-pentanetrione result in average diameters of 3 nm, whereas dimethyl-L-tartrate stabilizes 2.1 nm. X-ray diffraction and pair distribution function analysis were used to investigate the structural properties of the particles. TEM data confirm the individual particle size and crystallinity and show that the particles are agglomerated without structural coherence. Besides the introduction of these novel ligands for ZnO nanoparticles, we investigated, in particular, the influence of each synthesis step onto the final nanoparticle size in the powder. Previous studies often reported the employed synthesis parameters, but did not motivate the reasoning for their choice based on detailed experimental observations. Herein, we regard separately the steps of (i) the synthesis of the colloids, (ii) their precipitation, and (iii) the drying of the resulting gel to understand the role of the ligands therein. ZnO particles only covered with acetate grow to 5 nm during the drying process, whereas particles with any of the additional ligands retain their colloidal size of 2–3 nm. This clearly shows the efficient binding and effect of the presented ligands.

M. Zobel (✉) · H. Chatterjee · R. B. Neder (✉)
Department of Physics, Lehrstuhl für Kristallographie und Strukturphysik, Friedrich-Alexander University Erlangen-Nürnberg (FAU), Staudtstr. 3, 91058 Erlangen, Germany
e-mail: mirijam.zobel@fau.de

R. B. Neder
e-mail: reinhard.neder@fau.de

G. Matveeva · U. Kolb
Institut für Physikalische Chemie, Johannes Gutenberg-Universität, Jakob-Welderweg 11, 55128 Mainz, Germany

Introduction

Over the past decade, ZnO nanoparticles have become interesting candidates for many applications such as dye-sensitized solar cells (Anta et al. 2012; Rani et al. 2008), transistors (Klingshirn 2007), or UV light-emitting diodes (Vanmaekelbergh and van Vugt 2011; Singh et al. 2013). Non-aqueous sol–gel syntheses are suitable to produce nanoparticles <10 nm and have

hence been in the focus of innumerable studies. The syntheses are generally carried out in alcoholic solutions of zinc salts by adding a base. The original ZnO sol–gel recipe by Spanhel and Anderson (1991) produced particles of 3.5 nm in diameter from a zinc acetate dihydrate salt in ethanol, yet their particles grew to 5.5 nm within 5 days. Even though recent in situ studies detected particle species with sizes as small as 1.3 nm within reacting solutions (Wood et al. 2003), to our knowledge no study has been published that reports a straight-forward, room-temperature synthesis strategy for stable nanoparticle powders with particle sizes <5 nm. This reflects the intrinsic problem that unstabilized ZnO nanoparticles readily grow even in nominally dry powders, because the particles aggregate and then adsorbed water or surface hydroxyls serve as promoters for growth (Ali and Winterer 2010). Hydroxyl groups cover a good portion of the surfaces of ZnO particles produced via the sol–gel route based on zinc acetate salts (Kawska et al. 2008; Raymand et al. 2011). The remaining fraction of the surface is shielded by acetate molecules (Sakohara et al. 1998), which nevertheless cannot prevent the growth promoted by the hydroxyls.

Organic ligands are commonly used as stabilizers to produce nanocrystalline powders. For ZnO it was shown exemplarily that thiols can successfully decrease the growth rates and resulting particle sizes. Reproducibility and stability in powder form was, however, not discussed (Wong et al. 2001). Amine-capped ZnO particles as small as 2.3 nm were produced as powder via solvent evaporation of toluene, but the large drawback in this method is the total synthesis time of 5 days because of the slow evaporation (Kahn et al. 2005).

Consequently, it is worthwhile to look for a straight-forward synthesis strategy, which reproducibly results in nanoparticles of sizes below 5 nm with decent polydispersity and, in particular, good stability in their powder form. We optimized the synthesis parameters of a recipe at ambient conditions, which employs the organic base tetramethylammonium hydroxide to initiate ZnO nanoparticle formation in a 27 mM ethanolic solution of zinc acetate dihydrate (Wood et al. 2003; Music et al. 2002; Chory et al. 2007). Herein, we present a protocol of the influence of the individual steps of (i) the sol synthesis, (ii) the sol precipitation, and (iii) the drying of the gel onto the final nanoparticle size in the dry powder. The main influencing parameters in general are the stirring time of the sol and the precipitation procedure as well as for the case of pure acetate coverage the drying of the gel. We produced ligand-capped ZnO nanoparticles, which are rather stable for some weeks and do not change their size during the drying process. Particles capped with citric acid or 1,5-diphenyl-1,3,5-pentanetrione feature mean diameters of 3 nm and dimethyl-L-tartrate produces average sizes of 2.1 nm.

Materials and methods

Chemicals and synthesis

The synthesis procedure is based upon Spanhel and Anderson (1991) with changes as suggested by Wood et al. (2003); Music et al. (2002) and Chory et al. (2007). 0.59 g zinc acetate dihydrate ($Zn(CH_3COO)_2 \cdot H_2O$, >99 %) were dissolved in 100 mL anhydrous ethanol (99.5 %, <0.005 % H_2O) to yield a 27 mM solution at room temperature and ambient pressure. Together with the zinc acetate, either none or one additional organic ligand is dissolved at 6.75 mM. This solution is magnetically stirred for about an hour at room temperature. The organic ligands used are known to influence the shape and size of the final nanoparticles due to selective adsorption on certain crystal faces (Cornell and Schindler 1980; Liang et al. 2005; Neveu et al. 2002; Renuka et al. 1998; Zhang and Gao 2004). These are 1,5-diphenyl-1,3,5-pentanetrione (pent), dimethyl-L-tartrate (dmlt) and citric acid. The addition of the organic base tetramethylammonium hydroxide (TMAH, 25 wt% in methanol) at a ratio [TMAH]/[Zn^{2+}] = 2.7 initiates the formation of nanoparticles. For citric acid the ratio [TMAH]/[Zn^{2+}] is adjusted to 6, because of the acidic character of citric acid, which requires a larger amount of base to be added to adjust the pH equivalently. The particle formation and crystallization kinetics differ dependent on the ligand used and hence the different solutions have to be stirred for different times after base addition. In case of acetate, citrate, and pent 2 h of stirring are sufficient, whereas for dmlt the solution has to be stirred ca. 8 h. The subsequent addition of an antisolvent mixture of hexane and acetone (ratio 2.5:1) promotes the agglomeration of the previously suspended nanoparticles to white gel-like flocculates (Marczak et al. 2010). For the ligand pent, the flocculates form immediately, whereas for acetate and citrate a stirring time of 1–2 h is required and for

dmlt even 2 h or more. The flocculates are centrifuged twice with 900 rpm/125 rcf for 2 min and once with 3500 rpm/2000 rcf for 5 min, during which they sediment as a gel. In between the centrifugation steps, the supernatant is discarded and the sediment is washed with acetone to dissolve remaining ligand and unreacted precursor molecules from the gel. (20 mL of acetone are added to the sediment of 40 mL of initial sol.) The final sediment is dried overnight in a desiccator and pestled afterwards for its characterization via X-ray diffraction (XRD)/pair distribution function (PDF) analysis. All powders were produced according to this recipe if not specified otherwise in the text.

Solvents were obtained from either Roth or Sigma Aldrich. Zinc acetate dihydrate, 1,5-diphenyl-1,3,5-pentanetrione, and dimethyl-L-tartrate were purchased from Sigma Aldrich and citric acid bought from Roth. All chemicals were used without further purification.

All glassware, which was used for the synthesis, was cleaned with 1 wt% NaOH and 1 wt% HCl and rinsed three times with water and Millipore water and dried at 110 °C in a heating oven prior to usage.

Characterization

Laboratory powder X-ray diffraction

Lab XRD measurements were performed on an X'Pert powder diffractometer (Philips, Analytical, CuKα) at room temperature on standard powder sample holders. Scan times of the drying gels were short enough to minimize the drift of the background signal due to the evaporation of solvent from the wet gels and crumbling of the remaining gel chunks.

High-energy X-ray diffraction

Synchrotron XRD measurements were carried out at beamline ID-15-B at ESRF, Grenoble, with an X-ray energy of 56 keV, using a Perkin Elmer disordered silicon detector and at beamline 11-ID-B at APS, Chicago with an equivalent setup at 59 keV. The powder samples were measured in polyimide capillaries ($d_i = 1$ mm). The experiments were carried out at room temperature. In situ experiments were carried out on the reacting solutions after base addition for several hours without the addition of the antisolvent. The corresponding flow cell setup, experimental

details, and data analysis of the in situ data are reported elsewhere (Zobel et al.). The measurements were performed at room temperature and multiframe data sets were typically collected for 5 min for the powder samples and 1 min for the in situ data and averaged. Distance calibration was done with NIST CeO$_2$ standards.

Thermogravimetric analysis

Measurements of the powders were carried out in a TGA of type Q50 (TA Instruments) with a heating rate of 10 °C/min (Balance Gas Nitrogen 40 mL/min, Sample Gas Nitrogen 60 mL/min).

Transmission electron microscopy

TEM measurements were performed with Tecnai F30 at 300 kV equipped with a field emission gun and a Gatan Ultrascan 4000 CCD camera (4k $\times$ 4k) in TEM imaging mode. The samples were dispersed in ethanol and sprayed onto holy carbon coated TEM Cu-grids with an ultrasonic pulse (Mugnaioli et al. 2009). Due to agglomerates in the powders, a quantitative particle size distribution could not be generated.

Modeling

XRD data

Particle size information of the powders was extracted from the lab XRD data in two different ways. For the drying study of ZnO ac, Gaussian line profiles were fitted to the peaks and the Scherrer equation was used to extract particle size information from the (110) peak, which is the most reliable due to the least peak overlap. For high quality XRD data of ZnO-ac, ZnO-pent, and ZnO-dmlt, explicit modeling of the XRD data was performed. Atomistic models of nanoparticles were simulated and the powder diffraction pattern calculated via the Debye scattering formula within the DISCUS software package (Neder and Proffen 2009).

PDF data

Data reduction was done with Fit2D (Hammersley et al. 1995), PDF calculation with PDFgetX3 (Juhás et al. 2013). Fourier Transformation of the diffraction data results in the PDF, dubbed $G(r)$.

$$G(r) = \frac{2}{\pi} \int\limits_{Q_{\min}}^{Q_{\max}} Q[S(Q) - 1]\sin(Qr)dQ$$

$Q = 4\pi \sin(\theta)/\lambda$ is the wave vector transfer with the wavelength λ and the scattering angle 2θ. In the Fourier transformation the maximum accessible $Q_{\max} = 23$ Å^{-1} was used. An ensemble average of nanoparticles including stacking faults was created using the DISCUS software package according to the procedure described in Niederdraenk et al. (2011). Only the ZnO nanoparticles without organic ligands were refined, since the contribution of the ligand molecules is not visible in an X-ray PDF.

Results and discussion

Final particle size and storage stability

Wide angle X-ray or neutron scattering data reflect the diameter of structurally coherent particles. In the following, we describe the refinement of these diameters for our samples. Our TEM data confirm that the samples consist of individual nanoparticles, which form larger agglomerates. The TEM data do not show ZnO to ZnO core contacts or orientational correlation between neighboring particles. In the following text, particle size refers to this individual particle size.

In order to refine the particle size and crystallinity of the produced ZnO nanoparticles, high-energy XRD measurements with subsequent PDF analysis have been carried out. A significantly large number of powder samples have been produced for each of the ligands. The samples were pre-characterized on the lab source within 1 day after synthesis and used in various PDF beamtimes between 3 and 8 days after synthesis. The resulting PDFs were fitted with a model of monodisperse ellipsoids including stacking faults (stacking fault probability p_{stack}). Refinements of the powder PDFs did not produce satisfactory fit qualities because peaks at large r have not been described fully and hence the particle size is somewhat underestimated, see Fig. 1a for the ligand citrate. In order to account for the missing contributions at large r, a model is needed which covers a particle size range. The easiest distribution to be assumed is a Gaussian distribution. We are well aware that most nanoparticle syntheses produce lognorm-distributed particle sizes. However, the PDF is not ideally suited to determine polydispersity although the average particle size can be deduced (Korsounski et al. 2003). We want to point out that some attempts have been made to fit polydispersity in nanoparticle PDF data before (Howell et al. 2006; Kodama et al. 2006). Howell et al. (2006) fitted a normalized distribution to the data and compared the results with TEM data, whereas Kodama et al. (2006) fitted a distribution based on TEM measurements to the data. While the actual distribution of our nanoparticle
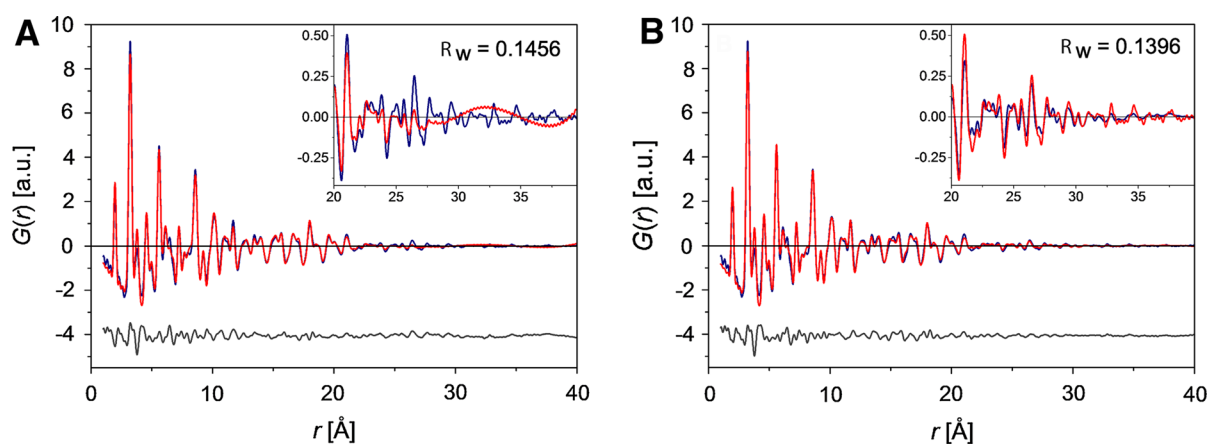

Fig. 1 Fit of monodisperse (**a**) and Gaussian distributed (**b**) nanoparticles to the experimental PDF of ZnO NPs with ligand citrate. The difference between the calculated (*red*) and the experimental (*black*) data is offset vertically to improve clarity. The Gaussian fit describes the data at large distinctively better, see *inset*. (Color figure online)

sizes is most likely a lognormal distribution as well, the quality of the refinement, as seen in Fig. 1 for the ligand citrate, justifies the application of the much faster and simpler application of a Gaussian distribution:

$$P(d_0, \sigma) = \frac{1}{\sqrt{2\pi\sigma^2}} \exp\left(-\frac{(d - d_0)^2}{2\sigma^2}\right)$$

In the distance range 20–40 Å, no significant differences remain which could be reduced by the use of a lognormal distribution, see inset Fig. 1b. The Gaussian fit describes the data significantly better compared to the monodisperse model (Fig. 1a), which is reflected by the improved R_w-value = 0.1396 in contrast to the R_w-value = 0.1456 for the monodisperse fit. Since the number of free parameters describing the particle size within the monodisperse ellipsoidal fit (d_{ab}, d_{cc}, p_{stack}) and the Gaussian fit of spheres ($d_{ab} = d_{cc}$, p_{stack}, σ) is identical, the Gaussian model is to be preferred.

Therefore, a Gaussian distribution was used to model the PDFs of the nanoparticles with the four different ligands, see Fig. 2.

The refinements yielded particle sizes, stacking fault probabilities and R_w-values as summarized in Table 1. ZnO can adopt either the cubic ($p_{stack} = 1$) or the energetically more favored wurtzitic phase ($p_{stack} = 0$). As the nanoparticle sizes decrease below 10 nm, the disorder within the particles increases, represented by the stacking fault probability. For the presented ZnO particles, it ranges from 0.13 for the 5.1 nm large ZnO-acetate particles up to 0.27 for the 2.1 nm ZnO-dmlt particles, which is comparable to so-far published values for other systems (Yang et al. 2013; Neder and Korsunskiy 2005).

In Fig. 2c and Table 1, it is readily seen that the fit of the ZnO-dmlt powder is slightly inferior to the other three refinements. This difference can be explained by inspecting the experimental PDFs. The full width half maxima (FWHM) of all ZnO-dmlt peaks are larger
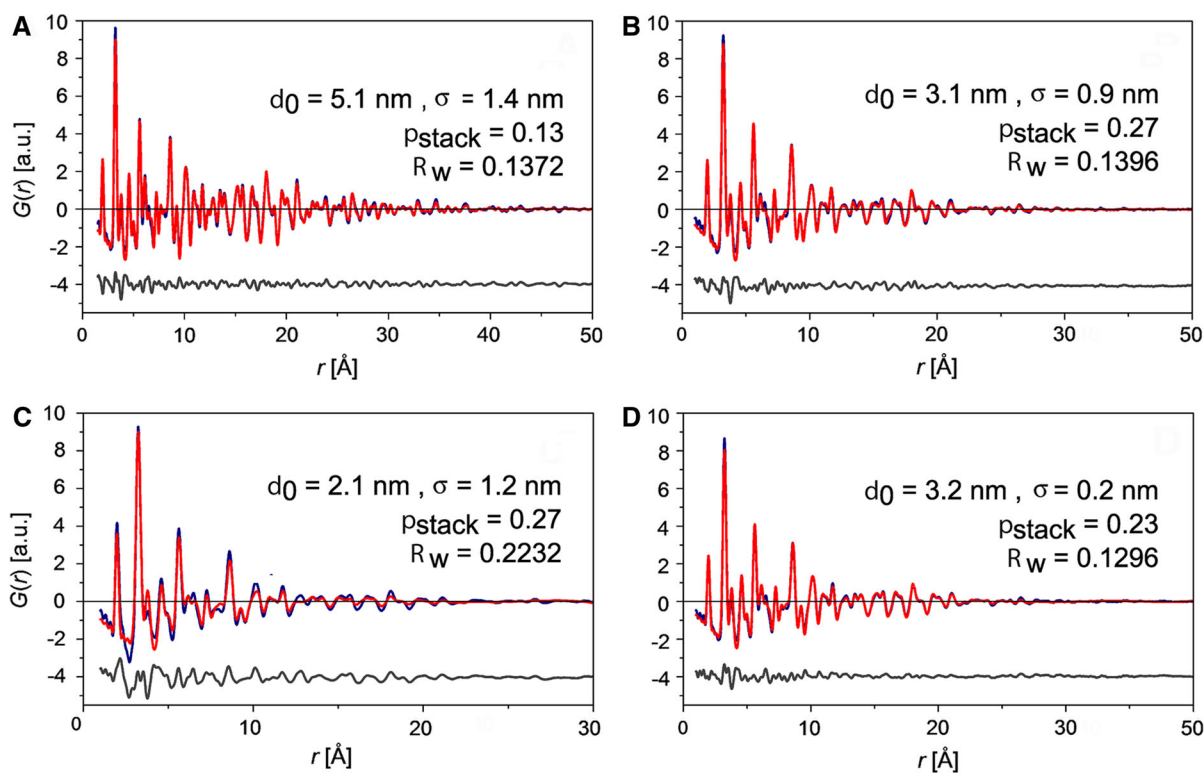

Fig. 2 Fits of nanoparticle powders with different ligand molecules: acetate (**a**), citrate (**b**), dimethyl-L-tartrate (**c**) and 1,5-diphenyl-1,3,5-pentanetrione (**d**). The difference between the calculated (*red*) and the experimental (*black*) data is offset vertically to improve clarity. (Color figure online)

Table 1 Fit results (mean diameters, width of Gaussian distributions and stacking fault probability) of nanoparticle powders together with R-values

Ligand	d_0 (nm)	σ (nm)	p_{stack}	R_w-value
acetate	5.1	1.4	0.13	0.1372
citric acid	3.1	0.9	0.27	0.1396
dmlt	2.1	1.2	0.27	0.2232
pent	3.2	0.2	0.23	0.1296

than those of all other ligands. Dmlt produces the smallest and most stable particles, which results from the strong binding of the dmlt molecule to the nanoparticle surface. It was shown for different nanoparticle systems, that the binding of adsorbents or ligands to the particle surface results in structural distortions of the perfect crystalline particle structure (Lei et al. 2014; Kaszkur et al. 2014; Gilbert et al. 2006). It is sensible to assume, that the dmlt molecules distort the wurtzitic ZnO structure, which enlarges the FWHMs of the PDF peaks. As this manuscript concerns the influence of synthesis conditions on the final nanoparticle size, a more detailed refinement model of ZnO-dmlt nanoparticles is not addressed herein.

The pre-characterization of the powders on the lab source directly after synthesis resulted in about the same particle sizes, calculated as rough estimates with the Scherrer equation. Additional detailed modeling of high quality lab XRD data using the Debye scattering equation to refine ellipsoidally shaped nanoparticles was also carried out. The refinements confirm the particle sizes from PDF and are shown in the Supporting Information, Figs. S1–S3. This indicates that indeed no significant growth can be observed within 1 week after synthesis and hence we achieved an increased stability of our nanoparticles within agglomerated powders in comparison with previous studies (Spanhel and Anderson 1991; Meulenkamp 1998b). The particle sizes and their crystallinity were further confirmed with high resolution TEM (HRTEM) measurements, as shown for ZnO-pent in Fig. 3, as well as for the other ligands in Figs. S4–S7 in the Supporting Information. The particles are agglomerated within the powders, but the individual nanoparticle size is in accordance with XRD and PDF results. Correctly oriented particles in the high resolution images of all samples exhibit the crystalline character of the particles.
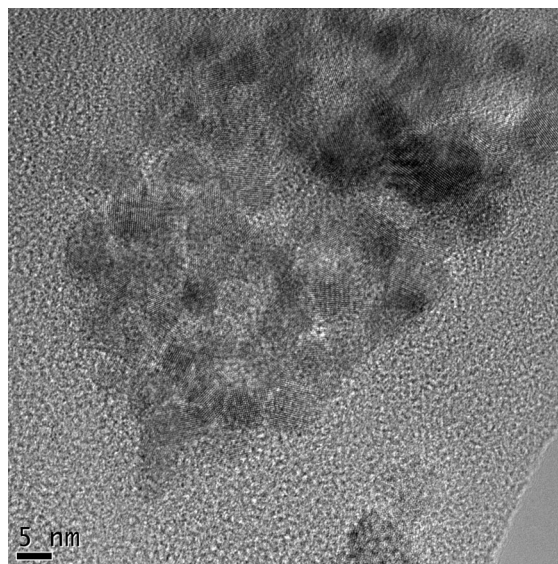
Fig. 3 HRTEM image of ZnO-ac nanoparticles

Furthermore, PDF measurements have been carried out several weeks up to 2 months after synthesis. The powders had been stored in glass vials with plastic caps at room temperature. The ligand pent proved to be the least stable. It degrades over time, which is directly observable by a color change of the powder from its characteristic shiny yellow to a pale yellow, see Fig. S8 in the Supporting Information. The particles tend to grow slightly within 1 week by a few Å, but increase their diameter significantly from 3.2 to 4.5 nm within 2 months. For pure ZnO nanoparticles such a growth is well known (Ali and Winterer 2010), and we also observe growth for our ZnO nanoparticles by about 1.5 nm. Particles stabilized with citric acid only grow by 1 nm in diameter during 2 months and dmlt-stabilized ones retain their size of ca. 2.1 nm. This goes hand in hand with the observation that the reaction kinetics of the synthesis of dmlt-stabilized particles are the slowest. Dmlt interacts the strongest with the zinc ions by complex formation in solution (Renuka et al. 1998; Cornell and Schindler 1980), which is reflected by the longest stirring times during synthesis. It also binds stronger to the nanoparticle surface, causing increased PDF peaks widths due to structural distortions within the particles, and hence produces the most stable particles sizes over extended periods of time.

Influence of synthesis parameters

The synthesis routine was optimized to gain small nanoparticle sizes by varying the base concentration, the amount of the organic ligands and the stirring times. The zinc concentration was given to be 27 mM by the solubility limit of $Zn(CH_3COO)_2 \cdot H_2O$ in ethanol at room temperature. The amount of organic ligand was varied from $n[ligand]/n[Zn^{2+}] = 0.14–0.25$, resulting in larger particles for lower concentrations. The smallest particles were observed for a ratio of 0.25 and further addition did not result in a further decrease of particle size. As observed multiple times before, the pH has to be adjusted to about 9 in order to initiate the reaction and to achieve sufficiently high supersaturation to gain small particles (Meulenkamp 1998b; Viswanatha et al. 2007; Hosono et al. 2004). Higher pH values favor the formation of zinc hydroxyl double salts and should be avoided (Tokumoto et al. 2003; Briois et al. 2007). The optimum pH corresponds to a ratio of [TMAH]/[Zn^{2+}] = 2.7 for acetate, pent, and dmlt. The ratio [TMAH]/[Zn^{2+}] = 6 for citric acid is higher, because of the acidic character of citric acid, which requires a larger amount of base to be added to adjust the pH equivalently.

Influence of precipitation and centrifugation

After the synthesis, the procedure of precipitation and centrifugation, including the washing of the gels, can alter the final crystallinity and yield of the nanoparticle powder. With the above centrifugation parameters in the Methods section, the produced powders consisted of pure wurtzite ZnO particles with no other crystalline or amorphous phases present. When the rotational speed or duration were lower, the yield of nanoparticle powder was smaller or no gel sedimented at all. Upon exceeding these parameters, too much organic residue (solvent and left-over ligands) were sedimented into the gel and observed as a wide, amorphous peak in the XRD patterns in the 2θ range of 10–30°.

The influence of the antisolvent mixture hexane–acetone and of the subsequent washing with acetone during the centrifugation steps onto the final powders was systematically studied. It was already known, that long alkane chains such as hexane are suitable to precipitate ZnO nanoparticles due to their antisolvent

effect (Meulenkamp 1998a; Marczak et al. 2010). Without agglomeration, the nanoparticles would stay suspended in solution. Acetone is an ideal solvent for organic molecules and added to the hexane in the antisolvent mixture to promote nanoparticle agglomeration due to the hexane and at the same time to dissolve left-over ligand molecules to gain pure ZnO powder without organic residues. Figure 4 shows the influence of these solvents onto the nanoparticle yield for the ZnO-pent system.

Without the addition of the antisolvent mixture, only very little sediment could be gained during centrifugation for solutions which had previously stirred 3 h. Upon washing these precipitates with acetone, they dissolved entirely and no sediment was formed with further centrifugation. Therefore, ethanol was tested as a washing solvent for the 3 h solution. The gained powder did not contain ZnO particles, but only consisted of amorphous residue (red curve, Fig. 4). The same solution was stirred for 16 instead of for only 3 h and then centrifuged and washed with ethanol, see green curve in Fig. 4. Now, ZnO particles were gained but accompanied by organic residue and with decreased overall yield. Quintupling the stirring times obviously enables the nanoparticles to form a certain amount of agglomerates even without the antisolvent addition. Hence, part of the same 16 h solution was washed with acetone instead of ethanol to
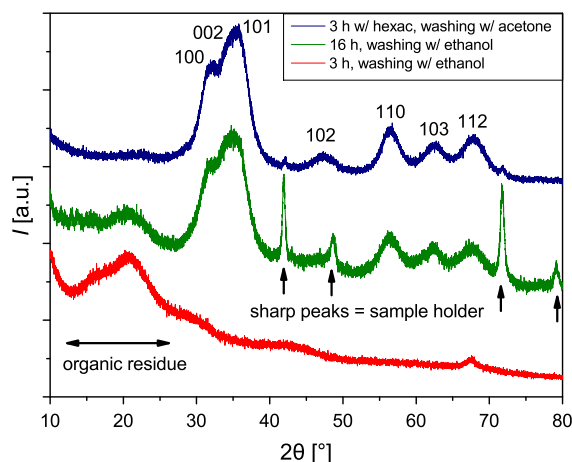

Fig. 4 Influence of precipitation and washing onto nanoparticle purity. Washing with ethanol does not reduce the amorphous residue (*red*, *green*) and centrifugation without previous precipitation shows smaller yield. Precipitation and acetone washing is required for phase-pure ZnO particles (*blue*). (Color figure online)

get rid of the organic residue. However, everything redissolved into solution upon the acetone addition and no powder could be gained at all. This shows, that the agglomerates formed upon quintupling of the stirring time are loosely bound and disintegrate due to the solvation power, which acetone exerts onto the organic ligand-capped ZnO particles.

In order to wash the ZnO agglomerates with acetone to get rid of the organic residues in the powders, precedent addition of an antisolvent is necessary to form compact agglomerates. The stirring time of the solution can at the same time be reduced to 3 h and phase-pure ZnO powders synthesized (blue curve, Fig. 4).

Influence of drying

After centrifugation, the nanoparticles are present in form of a gel, which is dried in a desiccator overnight. Not much attention has been given so far to the drying process as well as the correlation between particle sizes in the sols and in the final dry state (Marczak et al. 2010; Meulenkamp 1998b). From in situ experiments on the nucleation and growth of our ZnO sols, we know the particle size and crystallinity prior to the addition of the antisolvent for the systems described herein (Zobel et al.). The observed particles in the in situ experiments were also modeled with Gaussian distributed particle sizes and the fit results are shown in Table 2. It has to be pointed out, that the data quality of the highly diluted in situ samples is inferior to the powder data and hence R_w-values intrinsically higher. The accuracy of the determined particle size is therefore less precise than for the powders.

A comparison of Tables 1 and 2 shows that the particle sizes of the dry powders and in the sols match astonishingly well for dmlt. The nanoparticles in the

Table 2 Fit results (mean diameters, width of Gaussian distributions and stacking fault probability) of nanoparticle sols together with R-values

Ligand	d_0 (nm)	σ (nm)	R_w-value
acetate	2.2	0.4	0.2581
citric acid	2.3	0.6	0.2776
dmlt	2.2	0.5	0.3903
pent	2.0	0.6	0.2449

sol of citric acid and pent seem to grow somewhat during precipitation and drying, but a distinct effect is seen for acetate. Figure 5 compares the experimental PDF of the ZnO-acetate nanoparticles in the sol and in the corresponding dry powder. The size difference is readily seen, as significant PDF peaks (interatomic distances) appear in the distance range beyond 25 Å for the powder. Increasing the stirring times of the sols during the in situ experiments up to 14 h, did not increase the particle size in the sols at all. Hence, the growth has to occur during a post-synthesis step.

We carried out time-resolved XRD measurements of the drying process of the gels. Fresh samples were taken out of the desiccator at different times after centrifugation. The growth of the nanoparticles can be observed directly in the section of the diffraction patterns shown in Fig. 6 by the increase in peak height and decrease of FWHM. The particles grew from 4.5 nm in diameter for t = 5 min to 7.5 nm in the dry powder as estimated by the Scherrer equation from the FWHMs of fitted Gaussians. Times <5 min have not been accessible due to sample transfer time. This particle size increase explains the different particle sizes in the sols and powders. The slight mismatch of particle sizes as determined from the PDF fits ($d_0 = 5.1$ nm) and from the XRD patterns via the Scherrer equation ($d = 7.5$ nm) for the dry powder can be readily explained. Firstly, we fitted Gaussian-distributed particle sizes to the experimental PDFs, whereas the size from XRD was based on a
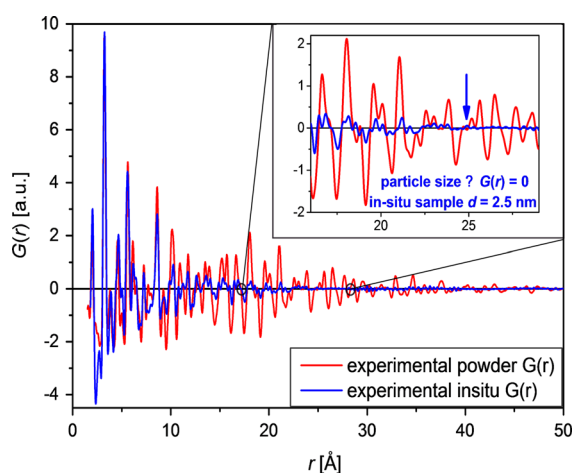

Fig. 5 Experimental PDF of dry ZnO acetate powder ($d_0 = 5$ nm) and ZnO sol in situ experiment after 14 h of stirring ($d_0 = 2.5$ nm). (Color figure online)
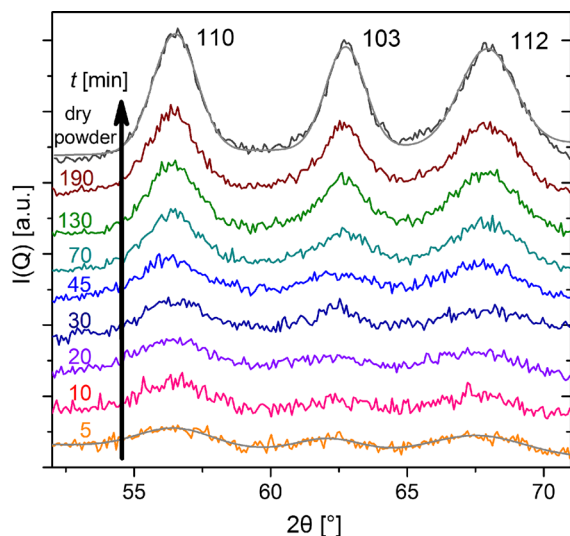
Fig. 6 Drying study of ZnO gel with ligand acetate. Part of diffraction pattern which was used for fit of particle size for t = 5, 10, 20, 30, 45, 70, 130 and 190 min as well as dry, pestled powder (from *bottom* to *top* as indicated by *arrow*) together with fit curves for t = 5 min and dry powder. (Color figure online)

Fig. 7 TGA measurement of ZnO-dmlt nanoparticles; whereas pure dmlt is decomposed entirely above 200 °C, the surface-bound dmlt on the nanoparticles partially stays on the particles up to 400 °C. The mass can be subdivided into the three regions of (*i*) evaporation of adsorbed solvent, (*ii*) decomposition of chemisorbed ligand and (*iii*) remnant of pure ZnO nanoparticles. (Color figure online)

monodisperse assumption. Moreover, by frequently taking out samples from the desiccator the drying conditions are not entirely identical, as the humidity in the desiccator is higher during this drying study compared to regular synthesis conditions. Water is known to contribute to post-synthesis particle growth (Ali and Winterer 2010) and this could also explain the difference in observed final particle sizes.

The most important consequence of this drying study boils down to the observation that our additional ligands citrate, pent, and dmlt successfully bind and stay on the nanoparticle surface during precipitation and centrifugation and strongly diminish the particle growth during the drying of the gel. We carried out TGA measurements to confirm the efficient ligand binding in the dry powders. The resulting mass loss is shown exemplarily for ZnO-dmlt in Fig. 7.

It has to be pointed out, that as-dried powders from the desiccator still possess some surface layers of solvent molecules such as hexane, acetone and ethanol, which only evaporate upon mild heating up to ca. 100 °C as indicated by the first region in Fig. 7. The second region and its corresponding mass loss up to shortly below 400 °C stems from the dmlt molecules, which are attached to the nanoparticle surface and represent ca. 30 % of the overall mass of

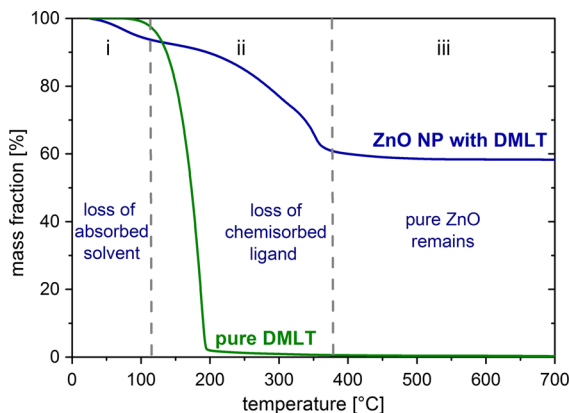the powders. Since pure dmlt decomposes above 150 °C entirely, see Fig. 7, it can be reasoned that the ligands are chemically bound to the nanoparticle surface, which increases their decomposition temperature. Above 400 °C only ZnO nanoparticles remain, which undergo growth at those elevated temperatures and in absence of stabilizing molecules. From the initial net weight and the average size of the nanoparticles, the weight loss attributed to the disintegration of dmlt can directly be converted to a surface coverage of 120 dmlt molecules per nanoparticle or 5.1 mol/nm^2. For pent, the coverage is 1.7 mol/nm^2, respectively, 40 pent molecules per nanoparticle. Both values lie in a typical range of surface coverages as recently studied in depth with NMR on similar systems (Valdez et al. 2014).

Conclusion

The known process of ZnO nanoparticle synthesis in alcoholic solutions via the sol–gel method has been modified to a simple, straight-forward recipe at room temperature. A detailed protocol of all essential parameters for the synthesis and subsequent precipitation and drying of the sols is given, with a focus on the change of the particle size and crystallinity within each step. Three organic ligands, namely citric acid, 1,5-diphenyl-1,3,5-pentanetrione and dimethyl-L-

tartrate are presented to stabilize ZnO nanoparticle powders to sizes well below 5 nm. The successful binding of the ligands was shown with TGA and their strongest influence onto the final particle size by the prevention of further growth during the drying of the gel. The synthesized ligand-capped powders show enhanced size stability over time, in particular, samples with dimethyl-L-tartrate do not grow perceivably for up to 2 months when stored as a powder at room temperature.

Conflict of interest   The authors declare no competing financial interests.

References

Ali M, Winterer M (2010) ZnO Nanocrystals: surprisingly "Alive". Chem Mater 22(1):85–91

Anta JA, Guillén E, Tena-Zaera R (2012) ZnO-based dye-sensitized solar cells. J Phys Chem C 116:11413–11425

Briois V, Giorgetti C, Dartyge E, Baudelet F, Tokumoto MS, Pulcinelli SH, Santilli CF (2007) In situ and simultaneous nanostructural and spectroscopic studies of ZnO nanoparticle and Zn-HDS formations from hydrolysis of ethanolic zinc acetate solutions induced by water. J Sol-Gel Sci Techn 39:3253–3258

Chory C, Neder RB, Korsunskiy VI, Niederdraenk F, Kumpf C, Umbach E, Schumm M, Lentze M, Geurts J, Astakhov G, Ossau W, Müller G (2007) Influence of liquid-phase synthesis parameters on particle sizes and structural properties of nanocrystalline ZnO powders. Phys Stat Sol (c) 4(9): 3260–3269

Cornell RM, Schindler PW (1980) Infrared study of the adsorption of hydroxycarboxylic acids on α-FeOOH and amorphous Fe (III) hydroxide. Colloid Polym Sci 258(10):1171–1175

Gilbert B, Zhang H, Huang F, Banfield JF, Ren Y, Haskel D, Lang JC, Srajer G, Jürgensen A, Waychunas GA (2006) Surface chemistry controls crystallinity of ZnS nanoparticles. Nanoletters 6(4):605–610

Hammersley AP, Svensson SO, Hanfland M, Fitch AN, Häusermann D (1995) Two-dimensional detector software: from real detector to idealised image or two-theta scan. High Press Res 14:235–248

Hosono E, Fujihara S, Kimura T, Imai H (2004) Non-Basic solution routes to prepare ZnO nanoparticles. J Sol–Gel Sci Techn 29(2):71–79

Howell R, Proffen T, Conradson S (2006) Pair distribution function and structure factor of spherical particles. Phys Rev B 73(9):094107

Juhás P, Davis P, Farrow CL, Billinge SJL (2013) PDFgetX3: a rapid and highly automatable program for processing powder diffraction data into total scattering pair distribution functions. J Appl Cryst 46:560–566

Kahn ML, Monge M, Collière V, Senocq F, Maisonnat A, Chaudret B (2005) Size- and shape-control of crystalline zinc oxide nanoparticles: a new organometallic synthetic method. Adv Funct Mater 15(3):458–468

Kaszkur Z, Rzeszotarski P, Juszczyk W (2014) Powder diffraction in studies of nanocrystal surfaces: chemisorption on Pt. J Appl Cryst 47(6):2069–2077

Kawska A, Duchstein P, Hochrein O, Zahn D (2008) Atomistic mechanisms of ZnO aggregation from ethanolic solution : ion association, proton transfer, and self-organization. Nanoletters 8(8):2336–2340

Klingshirn C (2007) ZnO: material, physics and applications. ChemPhysChem 8(6):782–803

Kodama K, Iikubo S, Taguchi T, Shamoto S (2006) Finite size effects of nanoparticles on the atomic pair distribution functions. Acta Cryst A62:444–453

Korsounski VI, Neder RB, Hradil K, Barglik-Chory Ch, Müller G, Neufeind J (2003) Investigation of nanocrystalline CdS-glutathione particles by radial distribution function. J Appl Cryst 36:1389–1396

Lei Y, Zhao H, Rivas RD, Lee S, Liu B, Lu J, Stach E, Winans RE, Chapman KW, Greley JP, Miller JT, Chupas PJ, Elam JW (2014) Adsorbate-induced structural changes in 1–3 nm platinum nanoparticles. J Am Chem Soc 136:9320–9326

Liang J, Liu J, Xie W, Bai S, Yu W, Quian Y (2005) Hydrothermal growth and optical properties of doughnut-shaped ZnO microparticles. J Phys Chem B 109:9463–9467

Marczak R, Segets D, Voigt M, Peukert W (2010) Optimum between purification and colloidal stability of ZnO nanoparticles. Adv Powder Technol 21:41–49

Meulenkamp EA (1998a) Size dependence of the dissolution of ZnO nanoparticles. J Phys Chem B 102:7764–7769

Meulenkamp EA (1998b) Synthesis and growth of ZnO nanoparticles. J Phys Chem B 102:5566–5572

Mugnaioli E, Gorelik T, Kolb U (2009) "Ab initio" structure analysis from electron diffraction data obtained by a combination of automated diffraction tomography and precession technique. Ultramicroscopy 109:758–765

Music S, Popovic S, Maljkovic M, Dragcevic D (2002) Influence of synthesis procedure on the formation and properties of zinc oxide. J Alloy Compd 347:324–332

Neder RB, Korsunskiy VI (2005) Structure of nanoparticles from powder diffraction data using the pair distribution function. J Phys Condens Matter 17:125–134

Neder RB, Proffen T (2009) Diffuse scattering and defect structure simulation. Oxford University Press, Oxford

Neveu S, Bee A, Robineau M, Talbot D (2002) Size-selective chemical synthesis of tartrate stabilized cobalt ferrite ionic magnetic fluid. J Colloid Interface Sci 255:293–298

Niederdraenk F, Seufert K, Stahl A, Bhalerao-Panajkar RS, Marathe S, Kulkarni SK, Neder RB, Kumpf C (2011) Ensemble modeling of very small ZnO nanoparticles. Phys Chem Chem Phys 13:498–505

Rani S, Suri P, Shishodia PK, Mehra RM (2008) Synthesis of nanocrystalline ZnO powder via sol–gel route for dye-sensitized solar cells. Sol Energy Mater Sol Cells 92:1639–1645

Raymand D et al (2011) Hydroxylation structure and proton transfer reactivity at the zinc oxide–water interface. J Phys Chem C 1010:8573–8579

Renuka R, Ramamurthy S, Muralidharan K (1998) Effect of citrate, tartrate and gluconate ions on the behaviour of zinc in 3 M NaOH. J Power Sources 76:197–209

Sakohara S, Ishida M, Anderson M (1998) Visible luminescence and surface properties of nanosized ZnO colloids prepared by hydrolyzing zinc acetate. J Phys Chem B 102:10169–10175

Singh P, Sinha OP, Srivastava R, Srivastava AK, Thomas SV, Sood KN, Kamalasanan MN (2013) Surface modified ZnO nanoparticles: structure, photophysics, and its optoelectronic application. J Nanopart Res 15:1758–1767

Spanhel L, Anderson M (1991) Semiconductor clusters in the sol-gel process: quantized aggregation, gelation, and crystal growth in concentrated ZnO colloids. J Am Chem Soc 113:2826–2833

Tokumoto MS, Pulcinelli SH, Santilli CV, Briois V (2003) Catalysis and temperature dependence on the formation of ZnO nanoparticles and of zinc acetate derivatives prepared by the sol-gel route. J Phys Chem B 107:568–574

Valdez CN, Schimpf AM, Gamelin DR, Mayer JM (2014) Low capping group surface density on zinc oxide nanocrystals. ACS Nano 8(9):9463–9470

Vanmaekelbergh D, van Vugt LK (2011) ZnO nanowire lasers. Nanoscale 3:2783–2800

Viswanatha R, Amenitsch H, Sarma DD (2007) Growth kinetics of ZnO nanocrystals: a few surprises. J Am Chem Soc 129:4470–4475

Wong EM, Hoertz PG, Liang CJ, Shi B-M, Meyer GJ, Searson PC (2001) Influence of organic capping ligands on the growth kinetics of ZnO nanoparticles. Langmuir 17:8362–8367

Wood A, Giersig M, Hilgendorff M, Vilas-Campos A, Liz-Marzán LM, Mulvaney P (2003) Size effects in ZnO: the cluster to quantum dot transition. Aust J Chem 56:1051–1057

Yang X, Masadeh AS, McBride JR, Bozin ES, Rosenthal SJ, Billinge SJL (2013) Confirmation of disordered structure of ultrasmall CdSe nanoparticles from X-ray atomic pair distribution function analysis. Phys Chem Chem Phys 15:8480–8486

Zhang J, Gao L (2004) Synthesis and characterization of nanocrystalline tin oxide by sol-gel method. J Solid State Chem 177:1425–1430

Zobel M, Neder RBN, Windmüller A, Milek T, Zahn D, Kimber SAJ, in preparation